# Reconstruction of precipitation $\delta$18O over the Tibetan Plateau since 1910

Jing Gao, Samuel S. P. Shen, Tandong Yao, Nancy Tafolla, Camille Risi, You He

AGU PUBLICATIONS

JGR

Journal of Geophysical Research: Atmospheres

RESEARCH ARTICLE
10.1002/2015JD023233

**Key Points:**
- An accurate representation of the spatiotemporal variation
- Valid reconstruction of precipitation $\delta^{18}O$ since 1910
- Successful $\delta^{18}O$ spectral optimal gridding

**Correspondence to:**
J. Gao,
gaojing@itpcas.ac.cn

**Citation:**
Gao, J., S. S. P. Shen, T. Yao, N. Tafolla, C. Risi, and Y. He (2015), Reconstruction of precipitation $\delta^{18}O$ over the Tibetan Plateau since 1910, *J. Geophys. Res. Atmos.*, *120*, 4878–4888, doi:10.1002/2015JD023233.

Received 10 FEB 2015
Accepted 28 APR 2015
Accepted article online 30 APR 2015
Published online 29 MAY 2015



# Reconstruction of precipitation $\delta^{18}O$ over the Tibetan Plateau since 1910

**Jing Gao[1,2], Samuel S. P. Shen[3,4], Tandong Yao[1,2], Nancy Tafolla[3], Camille Risi[5], and You He[1]**

[1]Key Laboratory of Tibetan Environment Changes and Land Surface Processes, Institute of Tibetan Plateau Research, Chinese Academy of Sciences, Beijing, China, [2]CAS Center for Excellence in Tibetan Plateau Earth Sciences, Beijing, China, [3]Department of Mathematics and Statistics, San Diego State University, San Diego, California, USA, [4]Scripps Institution of Oceanography, University of California San Diego, La Jolla, California, USA, [5]LMD/IPSL, CNRS, UPMC, Paris, France

**Abstract** An accurate representation of the spatiotemporal variation of stable isotopes in precipitation over the Tibetan Plateau (TP) is critical information for hydrological and ecological applications for the region. This paper reconstructs annual $\delta^{18}O$ data with 2.5° × 3.75° latitude-longitude resolutions over the TP since 1910 using the spectral optimal gridding (SOG) method. The SOG calculates empirical orthogonal functions (EOFs) from the Laboratoire de Météorologie Dynamique isotopic version general circulation model over the TP from 1978 to 2007 and regresses the $\delta^{18}O$ data of 10 ice cores over TP against the EOF basis functions. The reconstructed data can effectively demonstrate spatiotemporal characteristics of TP precipitation $\delta^{18}O$. The spatial average interannual $\delta^{18}O$ anomalies agree well with the time series of Guliya ice core $\delta^{18}O$, implying Guliya $\delta^{18}O$'s typical representation of the TP $\delta^{18}O$ temporal variation.

## 1. Introduction

The Tibetan Plateau (TP) is a "water tower" to a vast lowland region stretching all the way to the east coast of China and the south coast of India through majestic river systems, such as the Changjiang River and the Huanghe River as transmission pipes [*Immerzeel et al.*, 2010]. The TP encompasses the largest number of glaciers outside the polar regions [*Yao et al.*, 2012]. Detailed understanding of TP hydrological changes in a century time scale is critical to the future planning of hydrological and ecological projects and many other large-scale environmental designs for China, India, and their neighboring countries. However, there are no long-term observations from meteorological stations over the TP. We can only turn to illuminating the cause of past climate change using quantified climate proxies, such as precipitation $\delta^{18}O$. Correlation analysis between annual TP $\delta^{18}O$ data, the zonal index (ZI) and the South Asian summer monsoon index (SASMI), has shown that $\delta^{18}O$ reflects the South Asian climate [*Li and Zeng*, 2002; *Li and Wang*, 2003; *Yao et al.*, 2013]. An accurate representation of the spatial distribution of stable isotopes in precipitation can help quantify the TP spatiotemporal variations in precipitation [*Bowen et al.*, 2014]. Previous studies have demonstrated that the stable isotopes in precipitation are valid tracers to monitor the hydrological and climate changes in the TP [*Tian et al.*, 2003; *Yao et al.*, 2013], and the high-resolution ice cores provide direct records of past climates, offering a basic understanding of indirect archives via speleothems, lake sediments, or tree ring cellulose [e.g., *Danis et al.*, 2006; *Decelles et al.*, 2007; *Cai et al.*, 2010; *Henderson et al.*, 2010; *Grießinger et al.*, 2011; *Tan*, 2013].

The stable isotope compositions ($\delta^{18}O$ and $\delta D$) of precipitation over the TP exhibit spatial and temporal variations, the primary source of which is the Indian Ocean. The initial composition of Indian Ocean moisture is affected by evaporation and boundary layer mixing [*Boyle*, 1997; *Bowen and Revenaugh*, 2003]. When moisture is transported from the ocean to the continental regions, cooling and rainout occur continuously [*Dansgaard*, 1964], which results in compositional changes to the stable isotopes in precipitation. Generally, heavy isotopes decrease from ocean to inland. However, this decrease is not a simple function of their distance from an oceanic source, because moisture from other origins (e.g., locally evaporated moisture) or other processes (e.g., monsoon onset and topography lifting) affect the isotopic composition. Thus, the spatial distribution of stable isotopes in precipitation can have a complex spatiotemporal structure. For example, after the Indian monsoon onset, the $\delta^{18}O$ decreases immediately, reaching its lowest values in August in the southern TP, resulting in lower $\delta^{18}O$ values closer to the ocean, and higher $\delta^{18}O$ values inland TP [*Yao et al.*, 2013]. Thus, the spatial distribution of stable isotopes in

**Table 1.** Summary of 10 TP Ice Cores Used in This Study

| Ice Cores | Latitude (°N) | Longitude (°E) | Altitude (m) | Dating Period | References | Grid ID |
|---|---|---|---|---|---|---|
| Muztagata | 38.28 | 75.10 | 7010 | 1955–2000 | *Tian et al.* [2003] | 40 |
| Dunde | 38.10 | 96.40 | 5325 | 1910–1985 | *Yao et al.* [2006] | 44 |
| Malan | 35.83 | 90.67 | 5680 | 1910–1999 | *Wang et al.* [2006] | 35 |
| Guliya | 35.28 | 81.48 | 6200 | 1910–1992 | *Thompson et al.* [1997] | 24 |
| Puruogangri | 33.92 | 89.08 | 6070 | 1910–1994 | *Yao et al.* [2006] | 26 |
| Geladaidong | 33.34 | 91.18 | 5720 | 1935–2004 | *Kang et al.* [2007] | 27 |
| Tanggula | 33.12 | 92.08 | 5743 | 1910–2004 | *Joswiak et al.* [2010] | 26 |
| Noijinkangsang | 29.04 | 90.20 | 5950 | 1910–2006 | *Zhao et al.* [2012] | 9 |
| Dasuopu | 28.38 | 85.72 | 7200 | 1910–1996 | *Yao et al.* [2006] | 8 |
| East Rongbu | 27.98 | 86.92 | 6500 | 1910–1997 | *Hou et al.* [2003] | 8 |

precipitation reflects a combination of source effects and transport processes in the TP. In addition, the climate controls of precipitation $\delta^{18}O$ at the intraannual scale are different between the northern and the southern TP [*Gao et al.*, 2013]. Short-term $\delta^{18}O$ variation derived from only 1 or 2 years of data may bias estimates of long-term climatic variation [*Bowen and Revenaugh*, 2003]. Thus, these concerns highlight the need for methods that allow the long-term reconstruction of stable isotopes in precipitation from existing data sets [*Bowen et al.*, 2014]. IsoMAP cyber-GIS system that provides several unique capabilities related to generating space- and time-specific water isoscapes is a good framework for such prediction, but the functionality of the existing toolkit is limited in scope [*Bowen et al.*, 2014]. The purpose of this paper is to reconstruct the TP spatiotemporal variations in annual precipitation $\delta^{18}O$ back to 1910.

The spectral optimal gridding (SOG) method can fully utilize the information provided by general circulation models (GCMs) and observed data and yield an error estimate [*Shen et al.*, 2004, 2014; *Smith et al.*, 1998]. The GCM isotope output can help simulate coherent spatiotemporal patterns of the isotope field based on climate dynamics, while the ice core data can anchor these patterns to form gridded data. This specific research uses $\delta^{18}O$ data from Laboratoire de Météorologie Dynamique isotopic version (LMDZiso) from 1978 to 2007 to compute empirical orthogonal functions (EOFs) and 10 ice core $\delta^{18}O$ data to anchor the EOFs for every year back to 1910. Our SOG method is different from the conventional spatial interpolation method described in geostatistics textbooks, such as inverse distance weight and objective analysis [e.g., *Isaaks and Srivastava*, 1989]. The weights of these conventional statistical interpolations have little or no consideration of the spatial patterns of an observed field, and the resulting gridded data may miss dynamical model information, such as a significant inversion of $\delta^{18}O$ with respect to the distance from an ocean [*Liu et al.*, 2008], and yield a dynamically inconsistent gridded field. Our SOG gridding method uses the EOF patterns derived from GCM output, and hence, the SOG-gridded observational field is dynamically consistent with climate models and can avoid the aforementioned inversion problem. This dynamical model constraint improves the reliability of our gridded field for applications.

Section 2 of this paper introduces data and our method; section 3 describes EOFs and data gridding results; and finally, section 4 summarizes findings and gives perspectives for future research.

## 2. Data and Method

### 2.1. Ice Core Data

TP $\delta^{18}O$ data dating back to 1910 from 10 ice cores are available along the north to south transect of the TP (see Table 1 and Figure 1). All the ice cores are drilled at high elevation (more than 5300 m above sea level). We use the ice core data from 1910 in our reconstruction. All the ice core data have annual resolution and can help describe the TP $\delta^{18}O$ interannual variability. The ice core $\delta^{18}O$ anomalies and their statistical moments are calculated. The top three largest variances occur in the Muztagata, Guliya, and Pruogangri ice cores, while the smallest variance occurs in the Dasuopu ice core (see Figure 2a). Compared to the varied ranges of all ice core $\delta^{18}O$ anomalies shown in Figure 2a, the variances of ice core $\delta^{18}O$ anomalies in the northern TP have a larger range than those in the southern TP, which is more consistent than variances of precipitation over the TP [*Liu and Yin*, 2001; *Kang et al.*, 2010]. This may result from the different moisture origins and dominant controls of precipitation $\delta^{18}O$ in the southern and northern TP [*Yao et al.*, 2013]. In

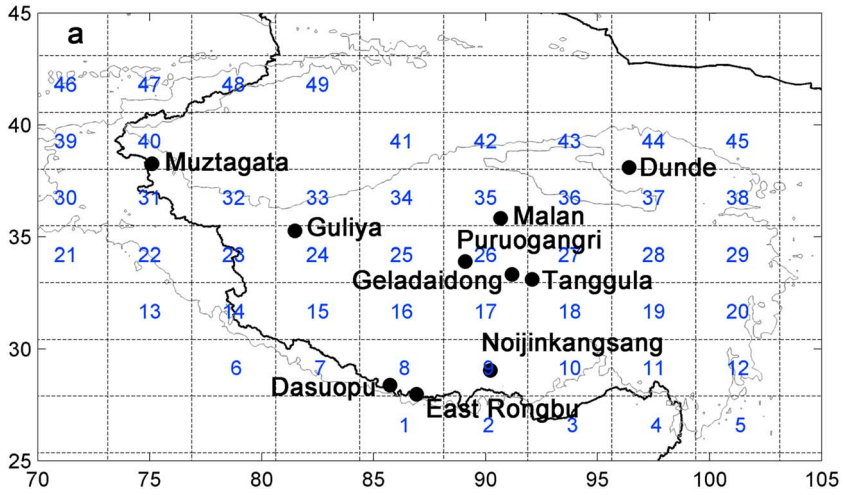


**Figure 1.** Locations of 10 TP ice cores, indicated by black round dots, and the grid of the LMDZiso simulation over the TP with a resolution of 2.5° × 3.75° latitude-longitude.

the northern TP, the local evaporation in hot and dry conditions brings mainly moisture with high $\delta^{18}O$ in summer, while the westerlies bring moisture with low $\delta^{18}O$ from far away in winter. Meanwhile, temperature controls the precipitation $\delta^{18}O$ variation at interannual and intraannual scales. However, in the southern TP, the summer monsoon brings major moisture with low $\delta^{18}O$, while the moisture comes from inland evaporation in cold and humid conditions or mixes with moisture transported far away with moderate $\delta^{18}O$. The summer monsoon also results in variations in precipitation $\delta^{18}O$ with changes of precipitation amount at daily and seasonal scales, but it disappears at the interannual scale. Interdecadal shifts of the ice core $\delta^{18}O$ anomalies exist in the southern TP.

The postdepositional processes that may lead to uncertainty and make age dating difficult are considered when each ice core is dated. These processes include the wind effect, surface snowmelting, sublimation, diffusion, and even reversal by the glacier movement [*Stichler et al.*, 2001; *Schotterer et al.*, 2004]. All the ice cores are drilled at very high elevation sites, where the low temperature prevents the surface from snowmelting. The increase in ice core density demonstrates that there is no reversal in the ice core, and the topographical evidence shows that no snow layers have overturned due to wind. Among these 10 ice cores, negligible postdepositional impact was estimated based on dating analysis [*Thompson*, 2000; *Tian et al.*, 2006; *Zhao et al.*, 2008].

### 2.2. LMDZiso Simulations

The $\delta^{18}O$ data from LMDZiso are used in this study to calculate EOFs. LMDZiso is the isotopic version of LMDZ, which is the atmospheric GCM developed by the Laboratoire de Météorologie Dynamique [*Hourdin et al.*, 2006], with a standard resolution of 2.5° × 3.75° and 19 vertical levels. The Van Leer advection scheme [*Van Leer*, 1977] is used in the model to calculate advected water in its vapor and condensed phases. Land surface evaporation is represented as a single flux in the model; e.g., there is no distinction between transpiration, bare soil evaporation, or evaporation of intercepted water by the canopy. *Hourdin et al.* [2006] described the model physical package in detail. The integration time step for the resolution of the large-scale dynamical equations is 1 min, and the physical package is called every 30 min. *Risi et al.* [2010] described the implementation of water stable isotopic processes. No fractionation is assumed during the evapotranspiration over land. To ensure a realistic simulation of the large-scale conditions, the sea surface conditions are forced by monthly observations following the Atmospheric Model Intercomparison Project (AMIP) protocol [*Gates*, 1992], and the simulated wind fields are relaxed toward the winds from the ERA-40 reanalyses [*Uppala et al.*, 2005] with a time step of 1 h [*Risi et al.*, 2010]. Here we use LMDZiso output at the monthly time step. It has been demonstrated that the LMDZiso simulations can successfully represent the spatial variations of the TP precipitation $\delta^{18}O$, but they underestimate the seasonal amplitude of $\delta^{18}O$ in the southern TP [*Gao et al.*, 2011]. This assessment makes the LMDZiso data particularly appropriate for our

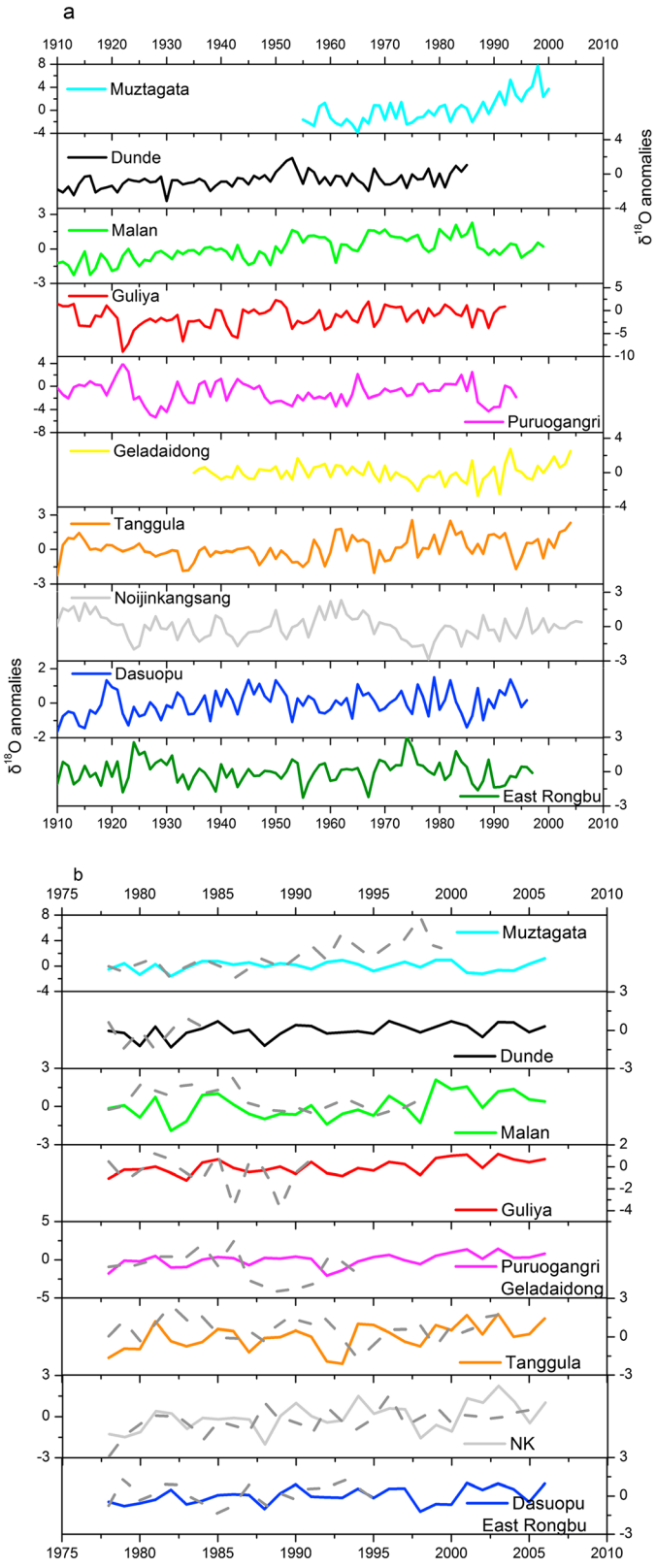


**Figure 2.** (a) Observed temporal series of annual $\delta^{18}O$ anomalies at 10 ice cores from 1900 to 2006. (b) Temporal series of $\delta^{18}O$ anomalies simulated by LMDZiso from 1978 to 2006, at the eight grids that include at least one ice core. The eight grid boxes are 8, 9, 24, 26, 27, 35, 40, and 44.

calculation of EOF, which is a set of spatial patterns. We use the annual LMDZiso precipitation $\delta^{18}O$ data with a resolution of 2.5° latitude × 3.75° longitude for the period of 1978–2007. The LMDZiso data set is a "nudged" simulation, using the AMIP protocol [*Gates*, 1992] and the European Centre for Medium-Range Weather Forecasts reanalysis data [*Uppala et al.*, 2005]. The TP region is covered by 49 grid boxes, numbered from north to south by grid ID (see Figure 1).

### 2.3. Model-Data Comparison

We compare the ice core data with LMDZiso output from the grid box, which includes the ice core. When a model grid box has more than one ice core, the grid box ice core data are an average of the ice core data. In this way, the 10 ice cores fall into eight grid boxes. LMDZiso simulates $\delta^{18}O$ anomalies well for some years, such as 1978, 1987, and 1991 at low ebb of $\delta^{18}O$ (Figures 2a and 2b), but it performs poorly in representing interannual variations in some southern grid points. Figure 3 displays the distribution characteristics of 10 ice core $\delta^{18}O$ anomalies during the 1978–2006 period. Fewer than 50% of $\delta^{18}O$ anomalies are negative. The $\delta^{18}O$ anomalies from −1‰ to 1‰ account for 63% of the total data, and the bulk of anomalies vary between −2‰ and 2‰.

The LMDZiso data have demonstrated a slight increasing trend since the late 1970s and noticeably underestimate the variances at Muztagata, Guliya, and Pruogangri (Figure 2b). The model simulation with the least variance of $\delta^{18}O$ anomalies shows at Dasuopu, where observed ice core $\delta^{18}O$ anomalies also show the smallest variance among the 10 ice cores. The simulated $\delta^{18}O$ anomalies demonstrate more asymmetrical patterns than the observed ice core $\delta^{18}O$ (Figure 3). Close to 45% of observed anomalies being negative, 48% of simulated anomalies are negative.

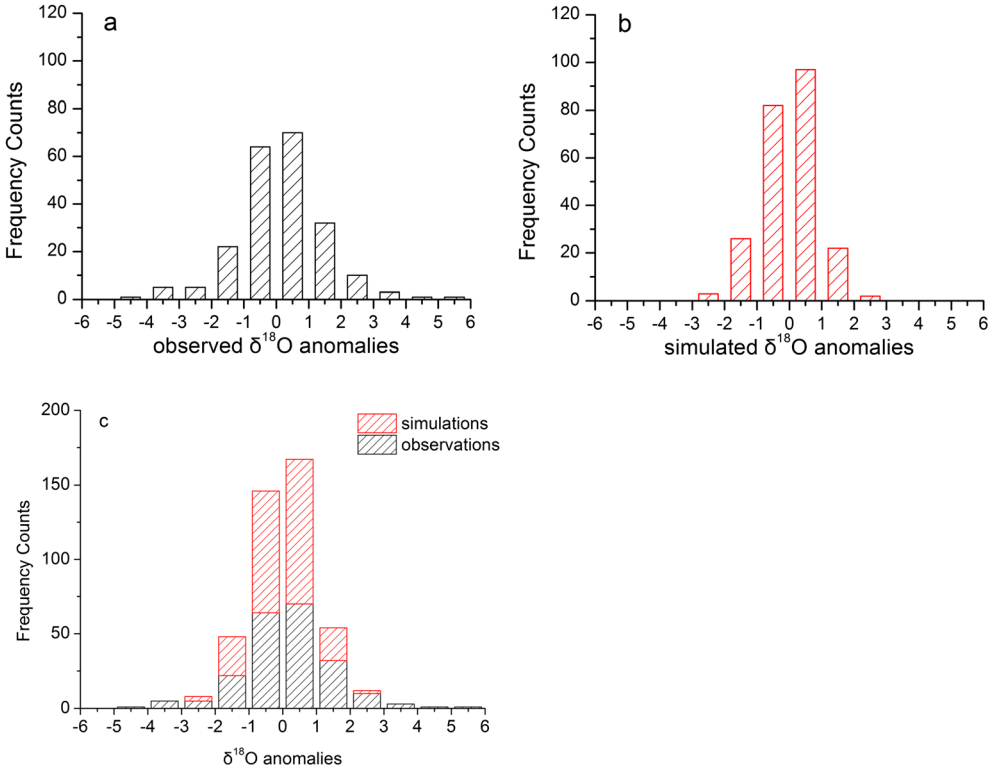


**Figure 3.** The histogram of 10 ice core $\delta^{18}O$ anomalies from (a) observations and the (b) LMDZiso simulations. (c) Comparison between observations and simulations. The black bar shows observations from 1978 to 2006, and the red bar shows LMDZiso simulations at the eight selected grid boxes from 1978 to 2006.

However, 42% of model anomalies are in (0, 1‰), while 33% of observed anomalies are in (0, 1‰). Table 2 compares observed and simulated $\delta^{18}O$ anomalies at concurrent grid boxes from 1978 to 2007 using an array of statistical indices: maximum, minimum, mean, standard deviation, skewness, and kurtosis. Simulations show smaller standard deviation, indicating weaker variability. The negative skewness at Puruogangri and Geladaidong indicates that the LMDZiso model underestimates the $\delta^{18}O$ at these two concurrent grid boxes mainly due to large negative anomalies. The smaller kurtosis values of simulations at Tanggula, Noijinkangsang, Dasuopu, and East Rongbu in the southern TP indicate the model's excessive dispersion. The LMDZiso simulations distinguish the difference in precipitation $\delta^{18}O$ between the westerlies and Indian monsoon correctly. They reproduce the north-south spatial distribution of $\delta^{18}O$, and successfully captures the seasonal patterns of $\delta^{18}O$ over the TP, i.e., the unimodal variation of $\delta^{18}O$ in the northern TP and the bimodal variation of $\delta^{18}O$ in the southern TP [*Gao et al.*, 2011; *Yao et al.*, 2013]. Our SOG method needs an orthonormal EOF basis and prefers correct spatial patterns. The model's systematic underestimations of the $\delta^{18}O$ values [*Gao et al.*, 2011; *Yao et al.*, 2013] do not affect our SOG interpolation. Thus, the LMDZiso simulations are appropriate for our EOF calculation and for illustrating spatiotemporal characteristics.

### 2.4. The Spectral Optimal Gridding Method

Our data analysis method used the spectral optimal gridding (SOG) method to populate the scarce observed $\delta^{18}O$ data from limited ice cores to the entire TP grid and then used the area-weighted average to calculate the spatial average of $\delta^{18}O$ anomalies for the entire TP region masked by the 49 grid boxes. SOG has two steps: the first is to calculate EOFs from model simulated or modern observed (say, by satellite) spatially complete data and the second is to regress the EOFs about the historical scarce observed data [*Shen et al.*, 2004, 2014; *Smith et al.*, 1998, 2013]. In this way, the historical scarce data are being populated. Our EOFs are calculated from the LMDZiso simulations over TP with a resolution of 2.5° × 3.75° latitude-longitude

**Table 2.** The Statistical Summary of $\delta^{18}O$ Anomalies at the 10 Ice Cores During 1978–2007[a]

| Ice Cores | No. | Minimum (‰) | Maximum (‰) | Standard Deviation | Skewness | Kurtosis | Grid ID |
|---|---|---|---|---|---|---|---|
| Muztagata | 23 (30) | −2.01 (−1.58) | 7.74 (1.18) | 2.33 (0.75) | 0.84 ± 0.48 (−0.42 ± 0.43) | 0.97 ± 0.93 (−0.73 ± 0.83) | 40 |
| Dunde | 8 (30) | −1.54 (−1.32) | 1.04 (0.73) | 1.00 (0.54) | −0.86 ± 0.75 (−0.95 ± 0.43) | −0.65 ± 1.48 (0.87 ± 0.83) | 44 |
| Malan | 22 (30) | −0.75 (−1.91) | 2.26 (2.10) | 0.85 (1.00) | 0.78 ± 0.49 (0.18 ± 0.43) | −0.24 ± 0.95 (0.87 ± 0.83) | 35 |
| Guliya | 15 (30) | −3.76 (−1.23) | 1.31 (1.17) | 1.55 (0.65) | −1.28 ± 0.58 (0.11 ± 0.43) | 1.13 ± 1.12 (−0.85 ± 0.83) | 24 |
| Puruogangri | 17 (30) | −4.30 (−2.05) | 2.51 (1.45) | 1.98 (0.82) | −0.09 ± 0.55 (−0.79 ± 0.43) | −0.72 ± 1.06 (0.78 ± 0.83) | 26 |
| Geladaidong | 27 (30) | −2.71 (−2.05) | 2.77 (1.45) | 1.31 (0.82) | −0.01 ± 0.45 (−0.79 ± 0.43) | 0.29 ± 0.87 (0.78 ± 0.83) | 26 |
| Tanggula | 27 (30) | −1.70 (−2.10) | 2.50 (1.77) | 0.98 (1.00) | −0.30 ± 0.45 (−0.27 ± 0.43) | −0.07 ± 0.87 (−0.29 ± 0.83) | 27 |
| Noijinkangsang | 29 (30) | −2.87 (−2.02) | 1.59 (2.25) | 0.88 (1.00) | −0.68 ± 0.43 (0.04 ± 0.43) | 1.92 ± 0.85 (−0.25 ± 0.85) | 9 |
| Dasuopu | 19 (30) | −1.40 (−1.23) | 1.50 (1.01) | 0.83 (0.62) | 0.06 ± 0.52 (−0.04 ± 0.43) | −0.75 ± 1.01 (−0.83 ± 0.83) | 8 |
| East Rongbu | 20 (30) | −1.63 (−1.23) | 1.78 (1.01) | 0.92 (0.62) | 0.32 ± 0.51 (−0.04 ± 0.43) | −0.48 ± 0.99 (−0.83 ± 0.83) | 8 |

[a]Values without brackets are for observations, and values within brackets are for GCM simulations. Grid ID shows the locations of data in Figure 1a, and No. means the number of years of each ice core used in the calculation.

from 1978 to 2007. The first 10 EOFs explain 90% of the total variance, equal to 36.4‰. We used these 10 EOFs $E_m(i)$ as our regression variables:

$$\hat{O}(i,t) = \sum_{m=1}^{M} b_m(t) E_m(i) \tag{1}$$

where $E_m(i)$ is the $m$th EOF at grid box $i$, $t$ denotes time, and $M$ is the total number of modes used in the regression reconstruction and is equal to 10 in our experiment.

The spatial average of $\delta^{18}O$ field is

$$\overline{O}(t) = \sum_{i=1}^{N} \hat{O}(i,t) \frac{A_i}{\sum_{j=1}^{N} A_j} \tag{2}$$

where $A_i = \sqrt{cos\phi_i}$ is the area factor of the $i$th grid box and $\phi_i$ is the latitude of the grid box's centroid.

Based on this method and its output data, the spatial and temporal variations of TP $\delta^{18}O$ since 1910 were analyzed.

## 3. Results

### 3.1. EOF Modes of the TP $\delta^{18}O$

EOF analysis was conducted on $\delta^{18}O$ simulations from LMDZiso to characterize covariability of the time series and investigate potential annual $\delta^{18}O$ associations (e.g., provenance, transport paths, and temperature effect) since 1978. EOF 1 of Figure 4a accounts for ~25% of the total variance in the precipitation $\delta^{18}O$ series. The scree plot (i.e., Figure 4g) of eigenvalues and their 95% confidence interval in Figure 4 were computed using North's rule of thumb [*North et al.*, 1982]. The confidence interval of the first eigenvalue does not include the second eigenvalue and vice versa. Thus, the first eigenspace is well separated from the rest and should have a dimension equal to one at 5% significance level. The first EOF is likely physically meaningful. EOF 1 is characterized by a north-south dipole. Figure 4a shows mostly positive EOF 1 loadings in the northern TP and negative in the southern TP. This north-south spatial pattern is consistent with the spatial distribution of summer (June to September, briefly, JJAS) precipitation $\delta^{18}O$ over the TP, suggesting that summer variability plays a primary role in the annual $\delta^{18}O$ [*Yao et al.*, 2013]. The largest values exhibit in the southwest TP along the Himalayas, suggesting that the $\delta^{18}O$ in this region has a common moisture source or similar atmospheric transport processes. The Indian monsoon is the dominant control of the moisture transport in the southern TP in summer. Monsoon brings masses of moisture from the Arabian Sea, Bay of Bengal, and the tropical Indian Ocean crossing the high Himalayas, then reaching the southern TP. During this transport, heavy isotopes deplete over the southern TP and are hard to reach the northern TP. The heavy isotopes over the northern TP are attributed to local evaporations and the moisture transported by the westerlies. Therefore, EOF 1 most likely represents the different summer moisture sources and transport paths from south to north [*Yao et al.*, 2013; *Tian et al.*, 2001].

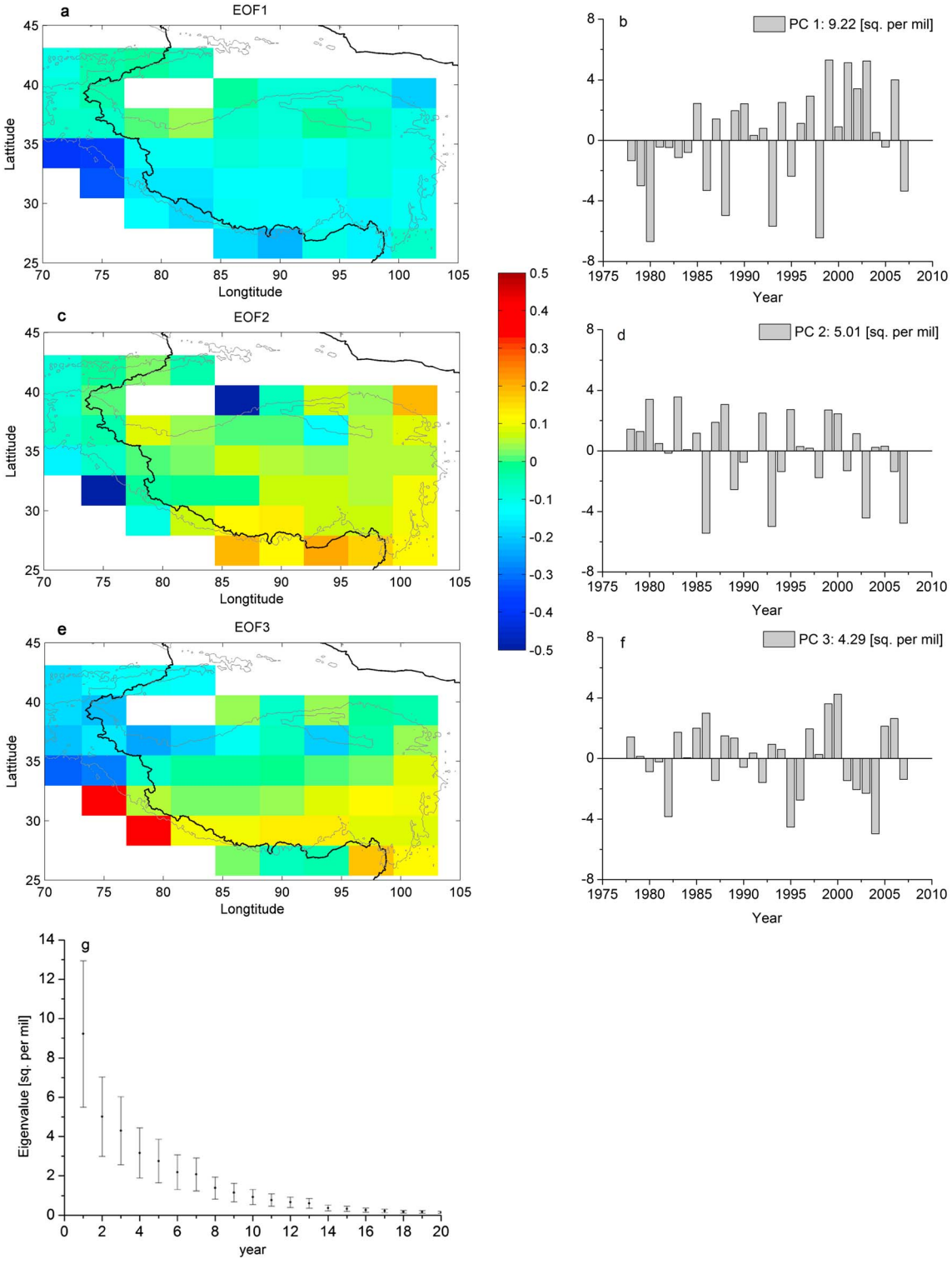


**Figure 4.** Results of the principal component analysis of the $\delta^{18}O$ anomalies simulated by LMDZiso from 1978 to 2007: (a, c, and e) spatial patterns of the first three EOF modes and (b, d, and f) time series of the respective principal components. The numbers in right legends show the eigenvalue for each PC. (g) Scree plot of the first 20 eigenvalues and their 95% confidence intervals.

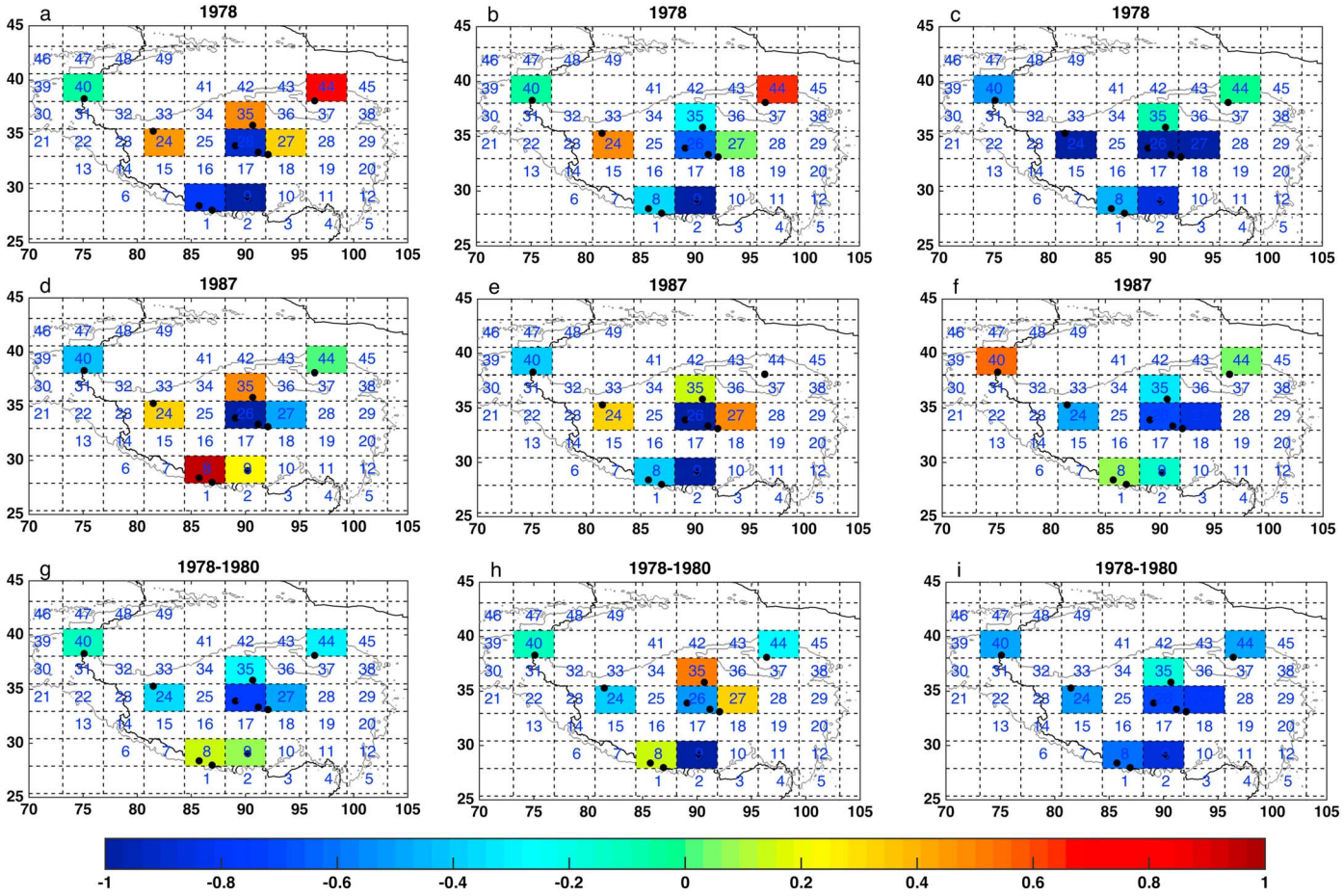


**Figure 5.** (a) Spatial distribution of TP average precipitation $\delta^{18}O$ anomalies in 1978 from reconstructions. (b) Same as Figure 5a but stands for observation. (c) Same as Figure 5a but stands for LMDZiso simulations. (d–f) Same as Figures 5a–5c but stand for 1987. (g–i) Same as Figures 5a–5c but stand for 1978–1980.

The scree plot of Figure 4g clearly shows that the eigenvalues of the second and third modes are not well separated. Thus, the eigenspace corresponding to the second and third eigenvalues may not be one dimensional, according to North's rule of thumb [*North et al.*, 1982]. The errors of EOF 2 and EOF 3 are large and comparable in size to the neighboring EOF, which implies that caution is needed to avoid overexplaining the physical meaning of EOF 2 or higher-order EOFs. Sometimes, a rotation of EOFs may help extract better, more physically meaningful results. However, the rotations we experimented with did not help and even mixed the nice north-south dipole property of the current EOF 1. We thus examined the unrotated EOFs to preserve the meaning of EOF 1. The EOF 2 of Figure 4c represents ~14% of the total variance in the annual $\delta^{18}O$ series. This spatial pattern shows positive loadings in the south and east TP, together with negative loadings in the north and west TP, opposite from that of EOF 1. The east-west dipole-like pattern of EOF 2 that conforms to the winter spatial pattern of precipitation $\delta^{18}O$ suggests that there may be different moisture transport in winter, which varied annually from the EOF 1 moisture transports. In winter, the westerlies are the dominant atmospheric circulation over the TP, transporting the primary moisture from far away. EOF 3 accounts for ~12% of the total variance and is of a large sampling error, again, according to North's rule of thumb [*North et al.*, 1982]. The largest values in the west suggest that there may be a secondary control of $\delta^{18}O$ variation in this region, distinct from other TP areas. The physical explanations of EOF 2 and EOF 3 are subject to further scrutiny due to their large sampling errors.

The time series of the corresponding principal components (hereafter PCs) are shown in Figure 4. PC 1, displaying the temporal behavior of EOF 1 mode, demonstrates the obvious interannual variation of $\delta^{18}O$ and clearly transition after 1998. Eight remarkable years appear for EOF 1, including 1999, 2001, 2003, and 2006 for the positive phase and 1980, 1988, 1993, and 1998 for the negative phase. The shifts of PC 2

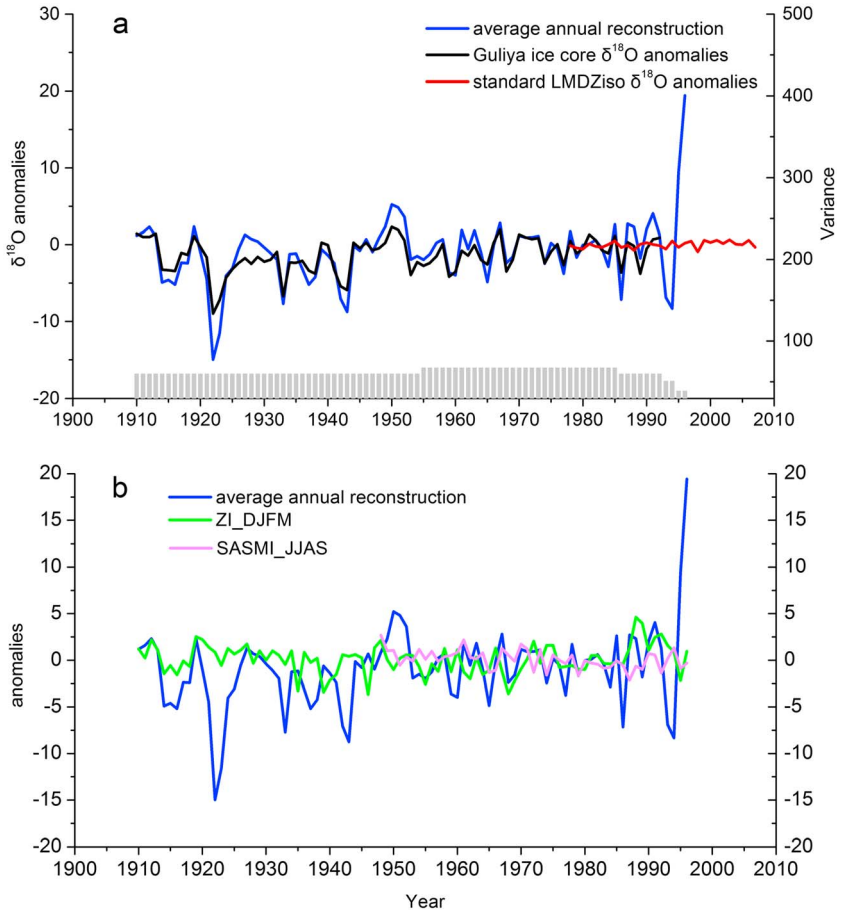


**Figure 6.** (a) Time series of reconstructed TP average annual precipitation $\delta^{18}O$ anomalies since 1910, compared with Guliya ice core $\delta^{18}O$ anomalies and simulated $\delta^{18}O$ anomalies from LMDZiso. (b) Comparison between reconstructed TP average annual precipitation $\delta^{18}O$ anomalies (blue) and DJFM zonal index (ZI, green) from 1910 to 1996, as well as JJAS South Asian summer monsoon index (SASMI, mauve) from 1948 to 1996.

remarkably increase after 1985 and show opposite trends with PC 1 from 1978 to 2007. This trend difference may be associated with the interannual variance of the westerlies and the Indian monsoon [*Yao et al.*, 2012; *Joswiak et al.*, 2013]. There is no apparent trend for PC 3, but the inflection points appear in 1982, 1986, 1995, and 2000 with distensible shift amplitude after 1995. Again, due to the large sampling errors, we refrain from overexplaining the physical meanings of PC 2 and PC 3.

In summary, the interannual variability of $\delta^{18}O$ simulated by LMDZiso features spatial coherence. The spatial characteristics of EOF 1 and EOF 2 are consistent with that of observed precipitation $\delta^{18}O$ in summer and winter, respectively. The EOF 1 and EOF 2 time series show apparent interannual variation and different trends. Although the physical meaning of an EOF with large sampling errors may become ambiguous, the errors do not affect the fact that the set of EOFs still forms an orthonormal basis for reconstructing the $\delta^{18}O$ data over the TP during the past century.

### 3.2. The $\delta^{18}O$ Reconstruction Over the TP

The comparison between reconstructions and observations/simulations at three specific durations (1978, 1987, and 1978–1980) is shown in Figure 5, due to low bias presented during these periods. The difference between observed ice core $\delta^{18}O$ anomalies and reconstructed $\delta^{18}O$ anomalies has a range between −1‰ and 0.1‰. The reconstruction reproduces the $\delta^{18}O$ anomalies in the western and eastern TP, compared with observations. However, it overestimates the varied amplitudes in the central and southern TP. In 1978, the largest difference is found in the central TP (grid boxes 26, 27, and 35), while in 1987, it moves to the southern TP (grid boxes 8 and 9). Considering the averages in 1978–1980, the remarkable differences exist in

both the central TP and the southern TP (grid boxes 9, 27, and 35). The difference between simulated ice core $\delta^{18}O$ anomalies and reconstructed $\delta^{18}O$ anomalies has a range between −1‰ and 2‰, larger than the difference with observations. Similarly, it reconstructs larger varied amplitudes in the central and northern TP in 1978 and 1987, remarkably, while the difference between simulations and reconstructions decrease in 1978–1980. In summary, the largest difference occurs in the central TP for both observations and simulations.

The averaged annual reconstruction over the TP accords well with the Guliya ice core ($R = 0.89$, $P < 0.01$; Figure 6a), except for the last 2 years. Larger variances are displayed during 1955 and 1985. However, simulations from LMDZiso appear too flat, although some annual shifts are consistent with observations. This demonstrates that the reconstruction can reproduce the characteristic interannual variation and spatial pattern of $\delta^{18}O$ anomalies over the TP. The abnormal values in the last 2 years may result from the overestimated weight function of the Muztagata ice core, which shows a remarkable increase of $\delta^{18}O$ after 1990.

The relationships between reconstruction and the annual ZI as well as the SASMI are analyzed to reveal the influence of the westerlies and the Indian monsoon on the $\delta^{18}O$ over the TP. ZI, defined as the normalized difference in zonal-averaged surface-level pressure anomalies between 35°N and 65°N, reflects the overall intensity of surface westerly anomalies over middle latitudes [*Li and Wang*, 2003]. For ZI, yearly averages are calculated from December to the following March (DJFM). No significant correlations are found between reconstruction over the entire TP and ZI, although the fluctuations match well from 1955 to 1973 (Figure 6b).

The SASMI, defined as an area-averaged summer (from June to September) dynamical normalized seasonality at 850 hPa within the 5°N–22.5°N and 35°E–97.5°E, reflects the interannual variation of the South Asian summer monsoon [*Li and Zeng*, 2002, 2005]. Yearly averages are calculated from June to September. The coincident shifts between reconstruction and SASMI exist during 1973–1984 (Figure 6b) but without significant correlations. This may indicate the coaction of the westerlies and South Asian summer monsoon on TP precipitation $\delta^{18}O$, but each plays a dominant role interlacing during different periods. More in-depth analyses are needed to compare with other GCM output and satellite data in the future.

## 4. Conclusions

We generated a $\delta^{18}O$ reconstruction on the TP at a resolution of 2.5° latitude × 3.75° longitude since 1910. The $\delta^{18}O$ interannual variability simulated by LMDZiso presents apparent spatial coherence. The modes of EOF 1 and EOF 2 seem to reflect the summer and winter precipitation $\delta^{18}O$ spatial patterns, respectively, relating to the interaction between the westerlies and the Indian monsoon. The gridded reconstruction successfully reproduces the observed spatial variation of the precipitation $\delta^{18}O$ anomalies. The obviously large differences between reconstructions and observations (observed ice cores) exist in central north TP. Similarly, the reconstructed interannual variation averaged on the TP fits with the Guliya ice core best since 1910.

The reconstruction of precipitation $\delta^{18}O$ has the potential to produce valid results in areas where no isotopic data were initially available and for periods when isotopic data were not available. The reconstruction can be used to provide input for stable isotopic hydrology models and as a template to interpret $\delta^{18}O$ archive records. A point of future work would be to improve the spatial resolution of the reconstruction and enhance the seasonal reconstruction.

**Acknowledgments**

This work was funded by the National Natural Science Foundation of China (grants 41471053 and 41190080), the "Strategic Priority Research Program (B)" of the Chinese Academy of Sciences (grant XDB03030100), and the IAEA Coordinated Research Project 17990/R0: Stable isotopes in precipitation and paleoclimatic archives in tropical areas to improve regional hydrological and climatic impact models. Shen was partly supported by the U.S. National Science Foundation (awards AGS-1015926 and AGS-1015957). LMDZiso simulations were performed on the IDRIS national computing center in France. The data of the ice core and the reconstruction are available by contacting Jing Gao (gaojing@itpcas.ac.cn). LMDZiso data are available by contacting Camille Risi (Camille.Risi@lmd.jussieu.fr). The suggestions from anonymous reviewers have helped improve the quality and clarity of this paper.

## References

Bowen, G. J., and J. Revenaugh (2003), Interpolating the isotopic composition of modern meteoric precipitation, *Water Resour. Res.*, *39*(10), 1299, doi:10.1029/2003WR002086.

Bowen, G. J., Z. Liu, H. B. Vander Zanden, L. Zhao, and G. Takahashi (2014), Geographic assignment with stable isotopes in IsoMAP, *Methods Ecol. Evol.*, *5*, 201–206.

Boyle, E. A. (1997), Cool tropical temperatures shift the global $\delta^{18}O$-T relationship: An explanation for the ice core $\delta^{18}O$-borehole thermometry conflict?, *Geophys. Res. Lett.*, *24*, 273–276, doi:10.1029/97GL00081.

Cai, Y., H. Cheng, Z. An, R. L. Edwards, X. Wang, L. Tan, and J. Wang (2010), Large variations of oxygen isotopes in precipitation over south-central Tibet during marine isotope stage 5, *Geology*, *38*(3), 243–246.

Danis, P. A., V. Masson-Delmotte, M. Stievenard, M. T. Guillemin, V. Daux, P. Naveau, and U. von Grafenstein (2006), Reconstruction of past precipitation $\delta^{18}O$ using tree-ring cellulose $\delta^{18}O$ and $\delta^{13}C$: A calibration study near Lac d'Annecy, France, *Earth Planet. Sci. Lett.*, *243*(3–4), 439–448.

Dansgaard, W. (1964), Stable isotopes in precipitation, *Tellus*, *16*, 436–468.

DeCelles, P. G., J. Quade, P. Kapp, M. Fan, D. L. Dettman, and L. Ding (2007), High and dry in central Tibet during the late Oligocene, *Earth Planet. Sci. Lett.*, *253*(3–4), 389–401.

Gao, J., V. Masson-Delmotte, T. Yao, L. Tian, C. Risi, and G. Hoffmann (2011), Precipitation water stable isotopes in the South Tibetan Plateau: Observations and modeling, *J. Clim.*, *24*(13), 3161–3178.

Gao, J., V. Masson-Delmotte, C. Risi, Y. He, and T. Yao (2013), What controls precipitation $\delta^{18}O$ in the southern Tibetan Plateau at seasonal and intra-seasonal scales? A case study at Lhasa and Nyalam, *Tellus B*, *65*, 21,043.
Gates, W. L. (1992), AMIP: The Atmospheric Model Intercomparison Project, *Bull. Am. Meteorol. Soc.*, *73*, 1962–1970.
Grießinger, J., Bräuning, A., Helle, G., Thomas, A., and G. Schleser (2011), Late Holocene Asian summer monsoon variability reflected by $\delta^{18}O$ in tree-rings from Tibetan junipers, *Geophys. Res. Lett.*, *38*, L03701, doi:10.1029/2010GL045988.
Henderson, A. C. G., J. A. Holmes, and M. J. Leng (2010), Late Holocene isotope hydrology of Lake Qinghai, NE Tibetan Plateau: Effective moisture variability and atmospheric circulation changes, *Quaternary Sci. Rev.*, *29*(17–18), 2215–2223.
Hou, S., D. Qin, D. Zhang, S. Kang, P. A. Mayewski, and C. P. Wake, (2003), A 154a high-resolution ammonium record from the Rongbuk Glacier, north slope of Mt. Qomolangma (Everest), Tibet-Himal region, *Atmos. Environ.*, *37*(5), 721–729, doi:10.1016/S1352-2310(02)00582-4.
Hourdin, F., et al. (2006), The LMDZ4 general circulation model: Climate performance and sensitivity to parameterized physics with emphasis on tropical convection, *Clim. Dyn.*, *27*(7–8), 787–813, doi:10.1007/s00382-006-0158-0.
Immerzeel, W. W., L. P. H. Beek, and M. F. P. Bierkens (2010), Climate change will affect the Asian water towers, *Science*, *328*, 1382–1385.
Isaaks, E. H., and R. M. Srivastava (1989), *An Introduction to Applied Geostatistics*, 561 pp., Oxford Univ. Press, Toronto.
Joswiak, D. R., T. Yao, G. Wu, B. Xu, and W. Zheng, (2010), A 70-yr record of oxygen-18 variability in an ice core from the Tanggula Mountains, central Tibetan Plateau, *Clim. Past*, *6*, 219–227, doi:10.5194/cp-6-219-2010.
Joswiak, D., T. Yao, G. Wu, L. Tian, and B. Xu (2013), Ice-core evidence of westerly and monsoon moisture contributions in the central Tibetan Plateau, *J. Glaciol.*, *59*(213), 56–64.
Kang, S., Y. Zhang, D. Qin, J. Ren, Q. Zhang, B. Grigholm, and P. A. Mayewski, (2007), Recent temperature increase recorded in an ice core in the source region of Yangtze River, *Chin. Sci. Bull.*, *52*(6), 825–831, doi:10.1007/s11434-007-0140-1.
Kang, S., Y. Xu, Q. You, W.-A. Flügel, N. Pepin, and T. Yao (2010), Review of climate and cryospheric change in the Tibetan Plateau, *Environ. Res. Lett.*, *5*(1), 015101, doi:10.1088/1748-9326/5/1/015101.
Li, J., and J. X. L. Wang (2003), A modified zonal index and its physical sense, *Geophys. Res. Lett.*, *30*(12), 1632, doi:10.1029/2003GL017441.
Li, J., and Q. C. Zeng (2002), A unified monsoon index, *Geophys. Res. Lett.*, *29*(8), 1274, doi:10.1029/2001GL013874.
Li, J. P., and Q. C. Zeng (2005), A new monsoon index, its interannual variability and relation with monsoon precipitation, *Clim. Environ. Res.*, *10*(3), 351–365.
Liu, X. D., and Z. Y. Yin (2001), Spatial and temporal variation of summer precipitation over the eastern Tibetan Plateau and the North Atlantic Oscillation, *J. Clim.*, *14*(13), 2896–2909.
Liu, Z., L. Tian, X. Chai, and T. Yao (2008), A model-based determination of spatial variation of precipitation $\delta^{18}O$ over China, *Chem. Geol.*, *249*, 203–212.
North, G., T. Bell, R. Cahalan, and F. Moeng (1982), Sampling errors in the estimation of empirical orthogonal functions, *Mon. Weather Rev.*, *110*(7), 699–706.
Risi, C., S. Bony, F. Vimeux, J. Jouzel, V. Masson-Delmotte, and F. Vimeux (2010), Water stable isotopes in the LMDZ4 general circulation model: Model evaluation for present day and past climates and applications to climatic interpretations of tropical isotopic records, *J. Geophys. Res.*, *115*, D12118, doi:10.1029/2009JD013255.
Schotterer, U., W. Stichler, and P. Ginot (2004), The influence of post-depositional effects on ice core studies: Examples from the Alps, Andes and Altai, in *Earth Paleoenvironments: Records Preserved in Mid- and Low-Latitude Glaciers*, edited by L. D. Cecil, J. R. Green, and L. G. Thompson, pp. 39–59, Kluwer Acad., Dordrecht, Netherlands.
Shen, S. S. P., A. N. Basist, G. Li, C. Williams, and T. R. Karl (2004), Prediction of sea surface temperature from the Global Historical Climatology Network data, *Environmetrics*, *15*, 233–249.
Shen, S. S. P., N. Tafolla, T. M. Smith, and P. A. Arkin (2014), Multivariate regression reconstruction and its sampling error for the quasi-global annual precipitation from 1900–2011, *J. Atmos. Sci.*, *71*, 3250–3268.
Smith, T. M., R. E. Livezey, and S. S. P. Shen (1998), An improved method for interpolating sparse and irregularly distributed data onto a regular grid, *J. Clim.*, *11*, 1717–1729.
Smith, T. M., S. S. P. Shen, L. Ren, and P. A. Arkin (2013), Estimating monthly precipitation uncertainty beginning 1900, *J. Atmos. Oceanic Technol.*, *30*, 1107–1122.
Stichler, W., U. Schotterer, K. Frohlich, P. Ginot, C. Kull, H. Gaggeler, and B. Pouyaud (2001), Influence of sublimation on stable isotope records recovered from high-altitude glaciers in the tropical Andes, *J. Geophys. Res.*, *106*(D19), 22,613–22,620, doi:10.1029/2001JD900179.
Tan, M. (2013), Circulation effect: Response of precipitation $\delta^{18}O$ to the ENSO cycle in monsoon regions of China, *Clim. Dyn.*, doi:10.1007/s00382-013-1732-x.
Thompson, L. G. (2000), Ice core evidence for climate change in the tropics: Implications for our future, *Quaternary Sci. Rev.*, *19*(1–5), 19–35.
Thompson, L. G., T. Yao, M. E. Davis, K. A. Henderson, E. Mosley-Thomson, P. N. Lin, J. Beer, H. A. Synal, J. ColeDai, and J. F. Bolzan, (1997), Tropical climate instability: The last glacial cycle from a Qinghai-Tibetan ice core, Science, *Science*, *276*(5320), 1821–1825, doi:10.1126/science.276.5320.1821.
Tian, L., V. Masson-Delmotte, M. Stievenard, T. Yao, and J. Jouzel (2001), Tibetan Plateau summer monsoon northward extent revealed by measurements of water stable isotopes, *J. Geophys. Res.*, *106*(D22), 28,081–28,088, doi:10.1029/2001JD900186.
Tian, L., T. Yao, P. F. Schuster, J. W. C. White, K. Ichiyanagi, E. Pendall, J. Pu, and W. Yu (2003), Oxygen-18 concentrations in recent precipitation and ice cores on the Tibetan Plateau, *J. Geophys. Res.*, *108*(D9), 4293, doi:10.1029/2002JD002173.
Tian, L., T. Yao, Z. Li, K. MacClune, G. Wu, B. Xu, Y. Li, A. Lu, and Y. Shen (2006), Recent rapid warming trend revealed from the isotopic record in Muztagata ice core, eastern Pamirs, *J. Geophys. Res.*, *111*, D13103, doi:10.1029/2005JD006249.
Uppala, S. M., et al. (2005), The ERA-40 Re-Analysis, *Q. J. R. Meteorol. Soc.*, *131*, 2961–3012.
Van Leer, B. (1977), Towards the ultimate conservative difference scheme: IV. A new approach to numerical convection, *J. Comput. Phys.*, *23*, 276–299.
Wang, N., T. Yao, J., Pu, Y. Zhang, and W. Sun, (2006), Climatic and environmental changes over the last millennium recorded in the Malan ice core from the northern Tibetan Plateau, *Sci. China Ser. D*, *49*(10), 1079–1089, doi:10.1007/s11430-006-1079-9.
Yao, T. D., et al. (2012), Different glacier status with atmospheric circulations in Tibetan Plateau and surroundings, *Nat. Clim. Change*, *2*, 663–667, doi:10.1038/NCLIMATE1580.
Yao, T. D., et al. (2013), A review of climatic controls on $\delta^{18}O$ in precipitation over the Tibetan Plateau: Observations and simulations, *Rev. Geophys.*, *51*, 525–548, doi:10.1002/rog.20023.
Yao, T., X. Guo, L., Thompson, K. Duan, N. Wang, J. Pu, B. Xu, X. Yang, and W. Sun, (2006), $\delta^{18}O$ record and temperature change over the past 100 years in ice cores on the Tibetan Plateau, *Sci. China Ser. D*, *49*(1), 1–9, doi:10.1007/s11430-004-5096-2.
Zhao, H., T. Yao, B. Xu, Z. Li, and K. Duan (2008), Ammonium record over the last 96 years from the Muztagata glacier in central Asia, *Chin. Sci. Bull.*, *53*(8), 1255–1261, doi:10.1007/s11434-008-0139-2.
Zhao, H., B. Xu, T. Yao, G. Wu, S. Lin, J. Gao, and M. Wang (2012), Deuterium excess record in a southern Tibetan ice core and its potential climatic implications, *Clim. Dyn.*, *38*(9–10), 1791–1803.